Lab on a Chip

PAPER

View Article Online
View Journal | View Issue

Cite this: *Lab Chip*, 2020, **20**, 1281

Low-frequency flexural wave based microparticle manipulation†

Hunter Bachman,[a] Yuyang Gu,[a] Joseph Rufo,[a] Shujie Yang,[a] Zhenhua Tian,[b] Po-Hsun Huang,[a] Lingyu Yu[c] and Tony Jun Huang *[a]

Received 22nd January 2020,
Accepted 28th February 2020

DOI: 10.1039/d0lc00072h

rsc.li/loc

Manipulation of microparticles and bio-samples is a critical task in many research and clinical settings. Recently, acoustic based methods have garnered significant attention due to their relatively simple designs, and biocompatible and precise manipulation of small objects. Herein, we introduce a flexural wave based acoustofluidic manipulation platform that utilizes low-frequency (4–6 kHz) commercial buzzers to achieve dynamic particle concentration and translation in an open fluid well. The device has two primary modes of functionality, wherein particles can be concentrated in pressure nodes that are present on the bottom surface of the device, or particles can be trapped and manipulated in streaming vortices within the fluid domain; both of these functions result from flexural mode vibrations that travel from the transducers throughout the device. Throughout our research, we numerically and experimentally explored the wave patterns generated within the device, investigated the particle concentration phenomenon, and utilized a phase difference between the two transducers to achieve precision movement of fluid vortices and the entrapped particle clusters. With its simple, low-cost nature and open fluidic chamber design, this platform can be useful in many biological, biochemical, and biomedical applications, such as tumor spheroid generation and culture, as well as the manipulation of embryos.

Introduction

Over the past several decades, microfluidics based platforms have been proposed and developed for many biological, biomedical, and industrial applications.[1–5] Offering improvements in cost, size, and precision, these tools have been regarded as potentially revolutionary for a litany of applications.[6,7] One specific application in which these tools have seen particular attention is the manipulation of micro and nano-sized materials or bio-specimen.[8–11] With the decreased dimensions of the microfluidic settings, researchers are able to probe and influence these small objects in previously unimaginable manners. Manipulation techniques that utilize fluids,[12–14] optics,[15,16] electronics,[17–19] magnetics,[20,21] or acoustics[22–25] have all been proposed and demonstrated. Of these tools, acoustic based manipulation methods can be advantageous in some applications, due to their high level of biocompatibility when working with fragile samples.[26] For example, researchers have utilized acoustics to concentrate micro/nano particles for numerous applications,[27,28] or for patterning/moving cells or particles for tissue engineering,[29–32] or analysis.[33–35] However, many of these systems rely on complex, high frequency acoustic transducers.[36,37] While these high frequencies improve the manipulation capability, they also complicate the operation of the device. Additionally, many acoustic based platforms manipulate particles in a closed chamber.[38] This closed design may keep the sample contained, but it limits the amount of interaction that the researcher can have with the sample. Additionally, the closed chamber may complicate the ability to culture, harvest, and analyze bio-samples after manipulation is complete. For this reason, researchers have recently begun exploring more 'open' microfluidic concepts.[39,40]

Herein, we present a low frequency flexural wave based acoustofluidic manipulation platform that can be used to pattern microparticles and cells within an open fluidic chamber. Flexural waves are bending waves which deform a material perpendicular to their propagation direction; in this work we explored the interaction of these waves with a fluid domain. With regards to the use of flexural waves in microfluidics, Nguyen and White previously explored the use of megahertz range flexural plate waves in the design of microfluidic pumping systems, although the performance

[a] *Department of Mechanical Engineering and Materials Science, Duke University, Durham, NC 27708, USA. E-mail: tony.huang@duke.edu; Tel: +919 684 5728*
[b] *Department of Aerospace Engineering, Mississippi State University, Starkville, MS, 39762, USA*
[c] *Department of Mechanical Engineering, University of South Carolina, Columbia, SC, 29208, USA*

† Electronic supplementary information (ESI) available. See DOI: 10.1039/d0lc00072h

achieved did not spur extensive interest.[41,42] The design of the device presented in this work is extremely straightforward relying on two inexpensive (~$1) commercial buzzers to actuate a thin glass slide and produce motion within the fluid domain. As a result of this vibration, particles which have fallen to the bottom surface of the glass substrate are concentrated at pressure nodes along the glass surface; additionally, rotational motion in the fluid domain can concentrate particles into rapidly rotating particle clusters. Notably, the dual transducer design of the device enables precise translation of the clusters central position. That is, with our device we are able to create stable fluid vortices and precisely manipulate their spatial positions. Both of these particle manipulation features are enabled by the flexural vibration of substrate of the device, which acts as a medium to carry the vibrational energy throughout the system. We believe that the simplistic, low-cost, and open nature of this platform offer it the potential to be used in biological and biomedical studies including the formation, and study of cell clusters and tumor spheroids,[43,44] as well as the manipulation of heavy bioparticles such as embryos. Additionally, the open nature of the fluid well makes the platform conducive to post-manipulation cell culture and analysis.

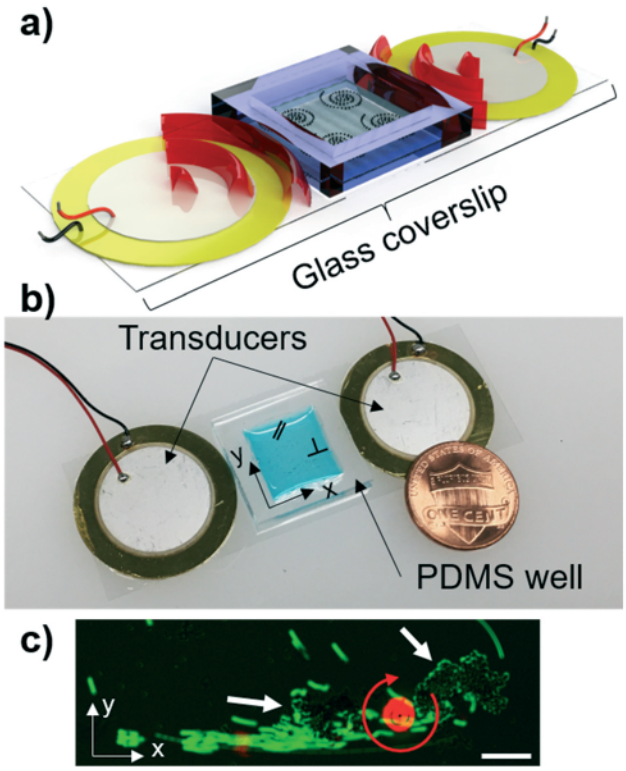

Fig. 1 (a) Schematic and (b) photo of the flexural-wave-based particle manipulation platform. The opposing transducers on either side of a glass coverslip create an interference pattern; adjusting the phase between the two signals enables translation of particle vortices in a controlled manner. The notations in the fluid region of (b) indicate the parallel (∥) and perpendicular (⊥) sides of the device for future discussion. (c) Stacked images showing the rotating particle group on the surface of the liquid (red), and particle group aggregating on the surface of the glass slide (green). Photo was taken along the parallel wall of the device. Scale bar: 500 μm.

Device mechanism

As seen in Fig. 1a and b, the flexural wave based acoustofluidic device utilizes a large glass substrate (25 × 75 mm) that can accommodate two transducers. Additionally, the fluid domain is constrained within an open fluid well. The walls of the chamber in Fig. 1b have been labeled with symbols to denote the parallel (∥) and perpendicular (⊥) sides of the device for future reference; namely, the parallel sides are in line with the x direction (primary direction of wave propagation), whereas the perpendicular walls are aligned with the y direction as noted in the figure. The dual transducers of the device are used to create an interference pattern on the glass substrate and within the fluid domain; actuating the transducers produces two different effects within the fluid domain depending on where an object of interest is located. That is, particles that have sank to the bottom of the fluid domain are concentrated at pressure nodes along the surface of the glass slide. However, particles that remain within the fluid domain are influenced by vortex streaming patterns that can also be used to concentrate the objects within the fluid domain. Both of these phenomena are shown in the composite image in Fig. 1c, where the red circle shows the rotating mass of particles (within the fluid domain), and the green portion of the image shows the particulates on the glass surface translating to a pressure node (marked by the white arrows). By selectively varying the phase difference between the excitation signals applied to each transducer, we are able to manipulate the microparticles in a controlled manner. Specifically, we are able to translate the particles on the glass substrate, and translate a fluid vortex within the fluid domain; manipulation of particle clusters trapped within the fluid vortex follow a precise relationship with the phase difference between transducer excitation signals.

We investigated the generation of wave patterns on the glass substrates of the device as a result of acoustic excitation of disc style transducers. Considering the commonly used operational frequencies (4–6 kHz), and materials (water: $c \approx 1495$ m s^{-1}, glass: $c \approx 5600$ m s^{-1}), the wavelengths of vibration within these devices would be expected to be on the order of hundreds of millimeters – much larger than the device itself. However, based upon the small dimensions of the glass substrate (~150 μm thick), the wavelength of flexural vibrations shrinks to the same scale as the device. The theoretical equation for the speed of sound of straight crested flexural waves in thin plates is given as:[45]

$$c = \left[\frac{Ed^2}{3\rho(1-\nu^2)}\right]^{\frac{1}{4}}\sqrt{\omega}, \quad (1)$$

where E, d, and ν, represent the Young's modulus, half-thickness of the thin plate, and Poisson's ratio, respectively.

Eqn (1) can be used to predict that the wavelengths of the vibration in this thin glass substrate should be approximately 17 mm in the frequency ranges that we traditionally utilize. This means that there could be multiple wave fronts occurring on the glass slide at the same time. As a result of this finding, we sought to determine if we could utilize an interference pattern between opposing vibrations to achieve a new method for particle manipulation. We began our investigation by exploring the effect of using two transducers to operate the acoustofluidic pump that was previously developed in our lab.[46] As a modification of this device, we bonded a second transducer to the bottom of the glass coverslip, as shown in Fig. S1.† Monitoring the pumping performance would offer us a simple strategy to demonstrate and explore the interactions of the transducer vibrations. In order to study the flow rate, we collected videos of particle motion in the channel using a fast camera and ImageJ software; this analysis showed that the decrease in the average flow rate in the channel followed a sinusoidal pattern as the phase difference between transducer excitations was varied (Fig. S1†). Considering this result, we moved forward to design a system based around a larger glass coverslip which could accommodate two transducers in an opposing orientation. The results that follow detail our experimentation with that device.

Materials and methods

Device fabrication

The design of the flexural-wave-based acoustofluidic device utilized in this experimentation is relatively simple compared to many other microfluidic platforms; that is, the open nature, and lack of microstructures inherently simplifies the design and fabrication of the system. Instead of relying on soft lithography to form a channel, we can simply cut our chamber by hand. For this device, an approximately 3.5 mm thick polydimethylsiloxane (PDMS) layer was fabricated by mixing Sylgard 184 silicone elastomer with its curing agent (Dow Corning) at 10 : 1 ratio. This mixture was cured in an oven at 65° for one hour before being cut to shape using a razor blade. The square chambers were cut from the PDMS with inner and outer dimensions of 15 and 20 mm, respectively. These PDMS squares were then bonded onto the surface of a 25 × 75mm glass coverslip (Cat. #72192-75, Electron Microscopy Sciences, USA), which has a thickness of approximately 150 μm. To enhance the bonding strength, the glass slide and the PDMS chamber were treated with air plasma (BD-10AS, ElectroTechnic Products, USA) before being aligned and pressed together. The combined coverslip and PDMS were then returned to the 65° oven for 24 hours to completely cure the polymer. After the second cure, the two piezoelectric transducers (AB2746B-LW100-R, PUI Audio, USA) were attached to opposite sides of the glass slide using epoxy (PermaPoxy™ 5 Minute General Purpose, Permatex, USA). Once the epoxy was cured, the device was ready for use.

Vibrometer measurement acquisition

In order to gain a better understanding of the wave patterns generated on the surface of the flexural-wave-based acoustofluidic device, we utilized a laser Doppler vibrometer (PSV-400, Polytec, Germany). This device analyzes Doppler shifts in a laser beam that is projected onto the surface of an object to characterize its vibration. In order to measure the vibration on the surface of the glass coverslip, the device was flipped over (to expose a flat surface without any PDMS or transducers on it), and sprayed with an aerosol powder (Spotcheck® SKD-S2 Developer, Magnaflux, USA) which is commonly used to detect defects using a penetrant. This spray makes it so that the laser from the vibrometer has an opaque surface to reflect off of for measurement. In order to improve the consistency of the vibration profile across devices (as well as the consistency of acoustofluidic manipulation performance), the device was fixed in a custom holder using scotch tape (Fig. S2†). The holder ensured that the device was secured in the same manner during each test, and this holder was utilized during all experimentation in the manuscript unless otherwise noted. Operation of the vibrometer consisted of defining the test area using computer software and defining the acoustic parameters of interest. Based off of the historical experimental performance of sharp-edge based devices, we chose to sweep the frequency range from 0 to 10 kHz. The oscillatory signal was generated by the vibrometer itself, and applied to the two transducers on the device through wire clips. In order to analyze the wave pattern when the signals were in phase, both positive wires of the transducers were connected to the same output of the vibrometer; to actuate the transducers in an out-of-phase manner, the negative of one transducer, and the positive of the opposite were connected to the same output. Once activated, the vibrometer automatically scanned the entire working area. We analyzed the output data using a custom Matlab script which enabled us to extract vibration amplitudes, and frequency spectra.

Numerical simulation setup

In order to gain a deeper understanding of the device performance, we created a custom numerical model using the finite element software Comsol Multiphysics®. The 3D model (Fig. S3†) consisted of a glass substrate, epoxy layers, two dual-layer piezoelectric transducers (brass and lead zirconate titanate), a PDMS well, and water. Utilizing the solid mechanics and electrostatics modules in combination with a piezoelectric multiphysics coupling, we were able to apply oscillatory voltages to the transducers and explore the wave patterns. The boundaries at the ends of the glass coverslip (covered with tape) were modelled as low-reflecting boundaries, which proved to yield comparable wave patterns to the experimental results. Using a frequency domain study, we could determine the wave pattern and vibration amplitude for a given set of input parameters.

Experimental operation of the flexural-wave-based acoustofluidic device

Experimental operation of the flexural-wave-based acoustofluidic device was simplified by using a dual channel function generator (AFG3022C, Tektronix, USA) to apply varying signals to the two transducers on the device. The function generator output is limited to 10 volts, which was sufficient to achieve functionality with the acoustic devices, and removed the added complexity of an additional power amplifier. Due to inconsistencies in device fabrication and assembly, the optimal frequency for each device varied slightly, as expected for a resonance based system. As such, we began testing in the center of the known working range (5 kHz), and would adjust the frequency applied to the transducers to identify the optimal signal. That is not to say that the device only works at a single frequency, but that there may be a peak in performance around a range where functionality is still achieved. As a result, it is still possible to define a single frequency for operation, and expect adequate performance from each working device. During testing, the device was secured using the custom holder (Fig. S2†) which was also built to fit onto the stage of a microscope. Microscope photos and videos were collected using an inverted microscope (Nikon) and either a fast camera (Photron), or a CCD camera (CoolSNAP HQ2, Photometrics, USA). Analysis of microscope data was completed using the open source software ImageJ, developed by the NIH. Throughout initial testing, it was found that having a hydrophilic interaction between the fluid domain and the chamber of the device improved device performance. As such, devices were treated with the air plasma for 10 seconds prior to experimentation using the high frequency generator to modify the surface of the device. It is well known that this treatment can significantly affect the hydrophobicity of PDMS,[47] and we found that the modified contact angle with the PDMS wall (Fig. S4†) contributes to the improved performance when compared to a hydrophobic interface. For testing, 400 μL of liquid was injected into the fluid chamber, to which 50 μL of the desired particle solution was added; this resulted in an approximate height of 2 mm for the fluid domain. This fluid volume was chosen because it sufficiently filled the channel without a risk of overflow; we did not notice a significant change in device performance when varying the height of the fluid, and the hydrophobicity of the chamber showed to be a much more influential factor in device functionality.

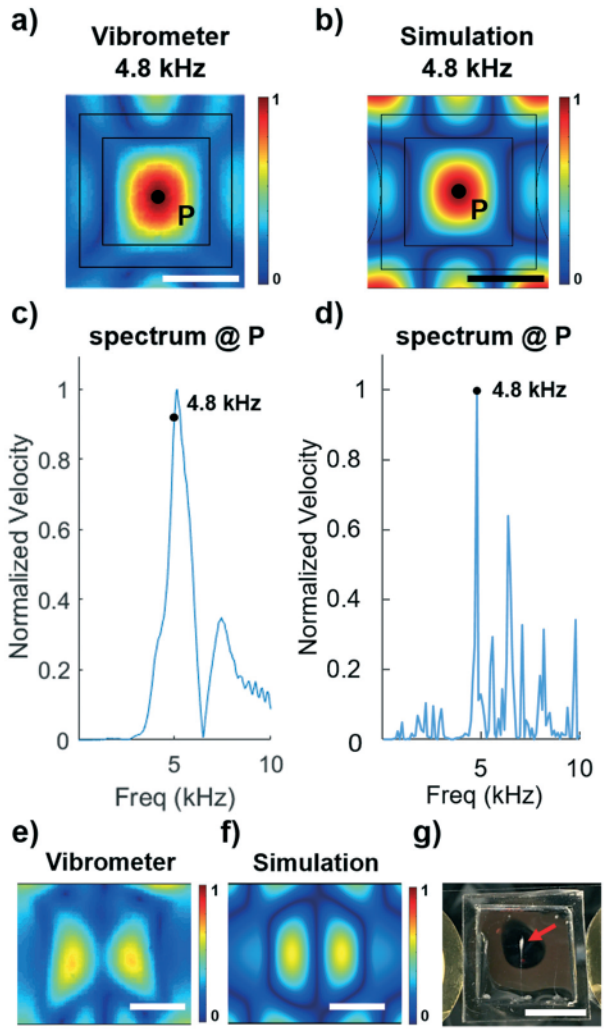

Fig. 2 (a) Experimental and (b) simulation results for the amplitude of vibration on the bottom surface of the flexural-wave-based acoustofluidic chip; vibration is the result of a 4.8 kHz in-phase excitation signal applied to both transducers. (c) Experimental and (d) simulation based plots showing the frequency response spectrum at the points P indicated in (a and b). (e) Vibrometer measurements and (f) numerical simulations of the vibration amplitude when the transducers were excited by 5.42 kHz signals which are out of phase. The vibrometer and simulation results show a clear pressure node located in the center of the chamber, consistent with the particle cluster seen in (g) our experimental observation. Colorbars indicate scale for each individual image. All scale bars: 10 mm.

Results and discussions

Vibration profile

We began our investigation by exploring the wave patterns generated on the surface of the glass slide using experimental and numerical methods. Utilizing the laser Doppler vibrometer and our custom Matlab script we were able to determine the experimental wave pattern on the bottom of the glass slide as shown in Fig. 2a, with the walls of the chamber superimposed on the image. The wave pattern shown was produced by a signal of 4.8 kHz applied to both transducers in-phase, and represents the magnitude of vibration throughout a period. We then compared this result to our numerical model (Fig. 2b) and noted that both results show a strong antinode in the center of the chamber. Notably, the model predicts slightly higher vibration amplitudes outside of the chamber, but the pattern within the chamber agrees with the vibrometer measurement. We further explored the experimental and computation domains by extracting the frequency response spectrum for each set of

data (Fig. 2c and d). Both the vibrometer collection and Comsol simulation predict a peak in the frequency response near the 5 kHz mark (vibrometer peak: 5.2 kHz, simulation peak: 4.8 kHz). As expected, the peak in the frequency response measured experimentally spans several frequencies from approximately 4–6 kHz; this is most likely caused by damping from the chamber and external connections, and is typical in a damped resonance system. The Comsol simulation, on the other hand, predicts sharper peaks, which decay rapidly. Notably, this may cause the amplitude predicted by the simulation to be lower than expected. Nonetheless, the overall response from both the simulation and experimental measurement are consistent with our prior experimentation with these flexural-wave-based acoustofluidic devices,[48,49] and provide use with a relative starting point for experimental determination of the optimal working frequency.

We next explored the vibration patterns when the excitation signals applied to the two transducers were out of phase. Fig. 2e and f provide the vibration amplitude profiles produced by the vibrometer measurement and simulation, respectively. As these results both show, a clear pressure node (low pressure line) located in the center of the channel, which is consistent with the experimental particle patterning shown in Fig. 2g. Additionally, we can utilize the distance between the pressure nodes in the channel to estimate the wavelength of the interference wave pattern; measuring these distances in Fig. 2e and f yields approximate wavelengths of 16.75 mm, and 17.2 mm for the vibrometer and simulation, respectively. These results are similar, and consistent with the expected wavelength calculated using eqn (1) (16.5 mm). As with any comparison between numerical and experimental results, subtle differences in the size of the glass slide or PDMS chamber, or alignment disparities between model and experimental device can contribute to errors between results; however, comparison presented here suggests that the model could be used as a qualitative tool for analyzing wave shapes and vibrational responses to guide experimentation. Using the data collected from the vibrometer, we were also able to visualize the propagation of waves across the surface of the glass slide, as shown in Video S1.† In these videos, we can see the wave patterns when the transducers were operated with signals that were both in phase, and out of phase. It can be seen that the in-phase wave pattern does not produce a particularly strong, or consistent node location, whereas the out of phase pattern maintains a lower pressure along the centerline. This is consistent with the vibration amplitude profiles for these instances (Fig. S5†), where the lack of localized low pressure fields relative to the pressure antinodes hinders particle concentration. That is, the wave pattern produced *via* the out of phase excitation signals is more conducive to particle patterning, as highlighted in Fig. 2g. If this platform were to be used for cell manipulation, the effect of the device on these organisms would be important. One common cause for concern with acoustic based manipulation is the undesirable generation of heat caused by transducer excitation; however, our previous experiments have shown that even under high power (50 volt excitation signal), the temperature of the transducer will not rise above 30 °C.[50] This means that heat generation should not be a concern for bio-sample manipulation.

Vortex based particle manipulation

While exploring the patterning of particles on the surface of the glass substrate, we noticed that the motion within the fluid domain was also serving to concentrate particles. Upon further inspection, we found that at the top of the fluid domain, near the surface of the water in the PDMS well, vortex streaming was created. Fig. 3 provides still images of the concentration process collected when both transducers had a 5.3 kHz, 10 V signal applied to them. As the figure shows, the 20 μm particles are drawn into the center of a vortex within 20 seconds of activating the transducers. We found that the vortex-based particle patterning and concentration was able to occur with only a single transducer being activated. However, we also found that the streaming velocity increased, and as a result the particle concentration

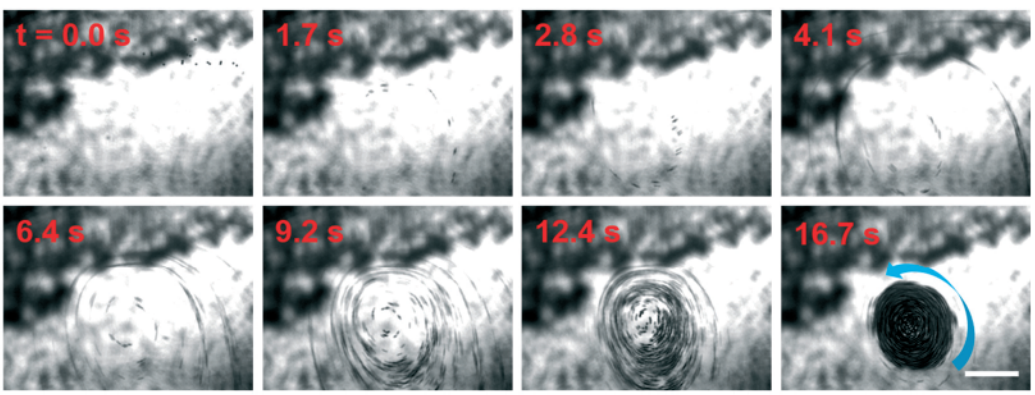

Fig. 3 Frames depicting the particle concentration effect in the acoustic vortex (20 μm particles) generated in the flexural-wave-based acoustofluidic device. Using a 5.3 kHz signal applied to both transducers, a rotating mass of particles has formed on the surface of the liquid in the device within 17 seconds. Scale bar: 500 μm.

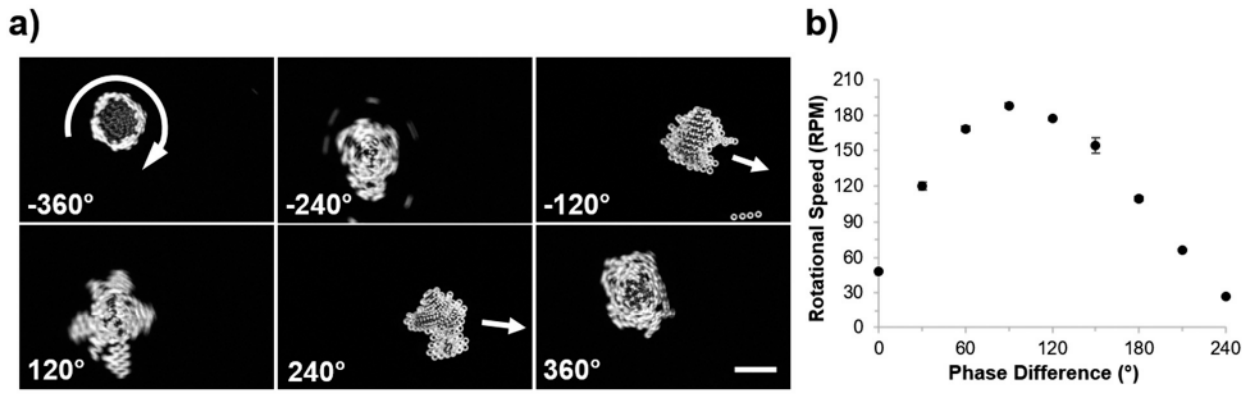

Fig. 4 (a) Stacked photos showing 25 μm particle rotation with various degrees of phase difference between the two transducer excitation signals; this particle mass was located along the perpendicular wall of the device, adjacent to the transducer (Fig. 1b). Varying the phase difference between the signals affected the rotation speed of the particle mass. 360 degrees apart (−120° and 240°), the particle group stopped rotating and started drifting to the side of the image before being brought back to rotating with a change of phase. Scale bar: 250 μm. (b) Plot showing the rotational speed of a separate group of particles; results were collected with a fast camera and analyzed using ImageJ. Results are consistent with the phenomenon in a), where the rotation speed varied based off of the phase angle. Data is shown ± one standard deviation for $n = 3$.

occurred more rapidly when both transducers were activated. Video S2† provides a side by side comparison of the particle concentration phenomenon when operating the device with a single transducer, or with both transducers. In our testing, the concentration occurred approximately twice as fast with the second transducer being active; this would be consistent with a constructive interference between the waves of the two transducers, creating a strong vibration, and more active vortex. Additionally, we would like to note that the vortex streaming was isolated to near the walls of the chamber, with multiple vortices being generated around the perimeter of the device, and the rotation direction of the different vortices alternated from clockwise to counterclockwise along a wall of the chamber.

We next tested the device's ability to concentrate particles with smaller diameters. Fig. S6† provides fluorescent images that show the particle concentration effect when utilizing 10 μm and 1 μm particles. We found that a small portion of 10 μm particles were able to be concentrated at the center of the vortex, but a larger portion simply follow the fluid streamlines in a circular pattern. Similarly, the 1 μm particles follow the circular streaming patterns, but do not concentrate. We believe that the concentration efficiency could be improved by utilizing a larger voltage signal, which could increase the streaming velocity, and the concentrating force on the particles as well.

Phase modulation and particle manipulation

Based off of our initial interest in using this technology as a tool for manipulation based on signal interference, we began to explore the effect of modulating the phase difference between the two transducers. We first analyzed the effect of a phase change on a particle cluster adjacent to the perpendicular wall of the chamber. A 5.56 kHz signal, with an amplitude of 10 volts was applied to both transducers, and a particle cluster concentrated along the wall. We fixed the phase of one of the output channels, and adjusted the phase of the second channel to produce a difference between the two signals. As we modulated the phase difference between the two signals, we noted that the rotation speed of the particle cluster varied; the photos in Fig. 4a provide a visualization of this phenomenon captured using the CCD camera. At specific phases in this device (−120° and 240°), the signals from the two transducer destructively interfered with each other to prevent rotation of the particle cluster. As one would expect, the two frequencies that produce this cancellation occur 360° apart from each other. At these points, the cluster began to drift away (noted by the white arrows), before being sucked back into the vortex upon its reformation at a new phase difference. Next, we quantitatively explored this cancellation effect using a fast camera and recording the rotation across a range of phase differences (Fig. 4b). The plot shown in Fig. 4b compares the rotation speed of the particle cluster to the phase difference, with a clear oscillatory response; that is, the rotation speed peaked at nearly 190 rpm with a phase difference of 90° between transducer excitation signals, and decreased away from this point; this is expected from the interference of two wave patterns, similar to the initial pumping experiment (Fig. S1†) Using the interference of the two transducer signals, it is possible to modulate the rotation speed of the particle cluster, and produce different forces on the particles within the mass.

Noting that these phase differences could affect the particle rotation along the perpendicular wall, we explored what would happen to the vortices along the parallel section of the device. We expected that since the wall was aligned with the general propagation direction of the waves, a phase change could potentially translate the particle vortex along the wall. As such, we focused our attention onto a vortex adjacent to the parallel wall, and began modulating the phase. Fig. 5a provides photos, while Fig. 5b provides a plot of the displacement of the rotating cluster along the parallel

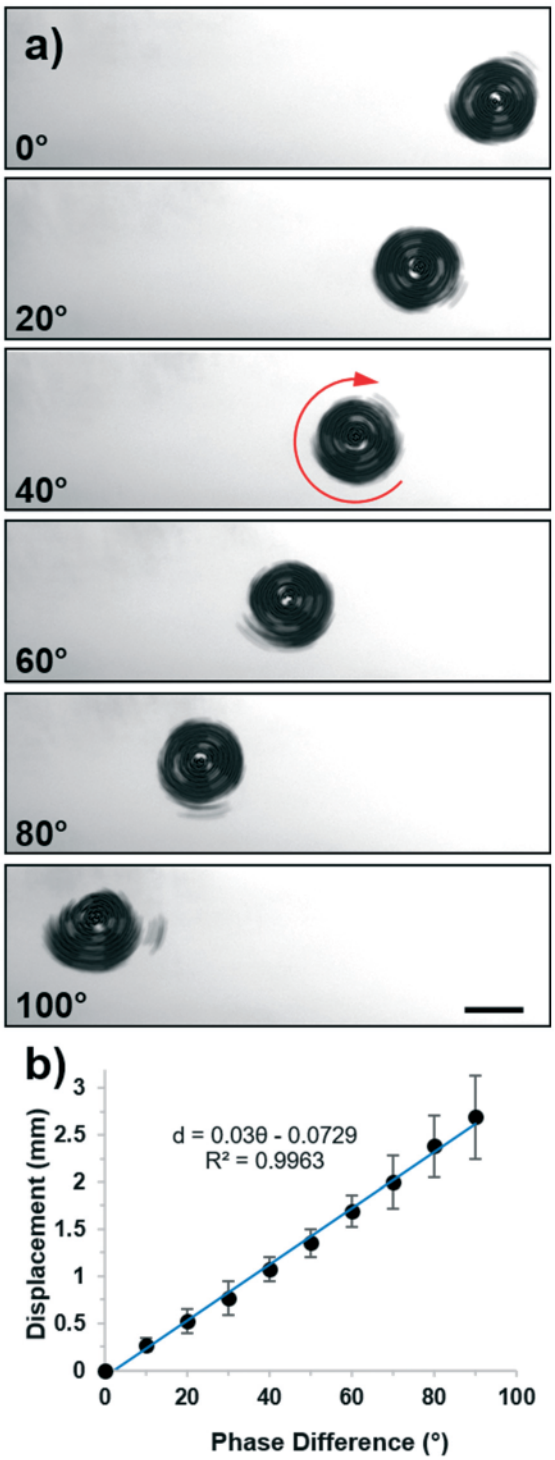

Fig. 5 (a) Microscope images showing the translation of the rotating particle group achieved by modulating the phase difference between transducer excitation signals. Results were collected along the parallel wall of the device (Fig. 1b), and showed a consistent translation as the phase change was modulated. Scale bar: 250 μm. (b) Plot showing the linear relationship between phase difference and translational distance. Data is shown ± one standard deviation for n = 4 samples, with a linear best fit of R^2 = 0.9963 included; the equation provided correlates the translational distance (d), as a function of the phase difference (θ) measured in degrees.

wall (a video of particle cluster rotation is provided in Video S3†). As we hoped, modulating the phase difference enabled us to vary the position of the rotating particle clusters. In fact, this particle translation was highly repeatable and linear in fashion, as would be expected from uniform standing wave fields utilized in other acoustofluidic devices.[38,51,52] We found that with the 5.42 kHz signal, the phase-dependent displacement was equal to an average of 30 μm deg^{-1}; we also used this data to calculate an apparent wavelength of 9.97 mm for the given frequency, which we found to be in disagreement with the wavelength prescribed by the straight crested flexural waves in eqn (1). However, this result is not unexpected based on the findings of Chen, *et al.* who explored the effect of coupled fluid layers on the surface of thin plates;[37] they found that a thin layer of water served as a pathway for energy to radiate from the vibration surface, which reduced the velocity of wave propagation, and the apparent wavelength of the signal.[53] Nonetheless, to verify this phenomenon, we returned to the study of particle patterning on the surface of the glass slide. Specifically, we compared the apparent wavelength of particle patterning on the glass substrate to the wavelength for phase manipulation of the vortex. Analyzing the particle patterning on the surface of the glass slide with an out of phase excitation pattern, we can actually see three node lines of particles in the fluid domain (Fig. S7†). Measuring the distance between these lines yields an apparent wavelength of 11.41 mm, which is similar to the 11.56 mm wavelength for the specific device which provided the comparison. Thus, it seems as though the vibration of the glass substrate, fluid domain, and the PDMS walls combine to form a complex flexural mode vibration which enables the particle manipulation; the fluid domain also serves to slightly reduce the wavelength when compared to the empty chamber testing we completed earlier. We further explored this phenomenon by measuring the phase-dependent displacement at another frequency; one would expect that a lower frequency would produce a larger wavelength. Analyzing the phase change for a 4.89 kHz excitations signal, we found that the apparent wavelength increased to 15.19 mm (Fig. S8†). This increase is consistent with the inverse relationship between the wavelength and square root of the frequency that is produced by eqn (1); that is, by manipulating eqn (1), we can arrive at the following wavelength–frequency relationship:

$$\frac{\lambda_1}{\lambda_2} = \sqrt{\frac{f_2}{f_1}} \tag{2}$$

The results of our study differ by only 3% (15.19 mm/4.89 kHz *vs.* 11.56 mm/5.42 kHz). This suggests that the mechanism of particle manipulation, although slightly shifted from the wavelengths predicted *via* eqn (1) due to fluid coupling, is a result of the flexural vibration of the system. Additionally, slight variations between numerical and experimental results can be explained by subtle

inconsistencies in device fabrication, component manufacturing, and experimental data collection.

As a final experiment, we explored the phase manipulation of 10 μm particles. Similar to our previous exploration, a small portion of the particles were concentrated, with the remainder of the particles following the streamlines (Fig. S9†). As we expected, the phase manipulation was still repeatable, with the concentrated cluster moving in a predictable and consistent manner; as the center of the vortex moved, the particles trapped in the outer streamlines translated to align with the new vortex center as well. This suggest that with a higher power, dense clusters of 10 μm objects could be formed and manipulated as well.

Conclusions

The flexural-wave-based acoustofluidic platform developed in this work presents a useful technology for particle and bio-sample manipulation. The inexpensive, mass-produced transducers utilized in this device, paired with its simplistic, open fluidic chamber design (no microstructures involved), offer a unique and inexpensive way for researchers to interact with samples. Throughout our investigation, we numerically and experimentally explored the wave patterns generated on the surface of the device, as well as the patterning of particles within pressure nodes on the glass coverslip. These pressure nodes can potentially offer researchers a way to form clusters of cells or embryos within the device. Additionally, we uncovered a unique potential to generate vortex streaming on the surface of the liquid in the device; this streaming enabled particle concentration and the dual transducer design allowed for precise control over the special location of the vortex. This capability could potentially be used to form cancer spheroids for biomedical research; the open chamber is also conducive to downstream culture and analysis of the patterned bio-samples. With future exploration, there is the potential to concentrate smaller particles, expanding the potential applications. Altogether, we have presented and characterized a simple, low-cost, open chamber platform for acoustofluidic manipulation, which has potential in many areas of research.

Author contributions

Conceptualization, H. B., and Z. T.; funding acquisition, T. J. H.; investigation, H. B., S. Y., J. R., and Z. T.; methodology, H. B., and Z. T.; project administration, P. H. H., Z. T., and T. J. H.; resources, S. Y., and T. J. H.; software, H. B., and Z. T.; supervision, T. J. H.; visualization, H. B. P. H. H, and Z. T.; writing – original draft, H. B.; writing – review & editing, H. B., P. H. H., Z. T., J. R., and T. J. H.

Conflicts of interest

No conflicts to declare.

Acknowledgements

We acknowledge support from the National Institutes of Health (R01GM132603, UG3TR002978, R01HD086325, and R01GM135486), United States Army Medical Research Acquisition Activity (W81XWH-18-1-0242), and National Science Foundation (ECCS-1807601).

References

1 H. A. Stone and S. Kim, *AIChE J.*, 2001, **47**, 1250–1254.
2 D. J. Beebe, G. A. Mensing and G. M. Walker, *Annu. Rev. Biomed. Eng.*, 2002, **4**, 261–286.
3 K. I. Ohno, K. Tachikawa and A. Manz, *Electrophoresis*, 2008, **29**, 4443–4453.
4 G. M. Whitesides, *Nature*, 2006, **442**, 368–373.
5 T. A. Franke and A. Wixforth, *ChemPhysChem*, 2008, **9**, 2140–2156.
6 T. D. Rane, H. C. Zec, C. Puleo, A. P. Lee and T. H. Wang, *Lab Chip*, 2012, **12**, 3341–3347.
7 J. Zhang, S. Yan, D. Yuan, G. Alici, N. T. Nguyen, M. Ebrahimi Warkiani and W. Li, *Lab Chip*, 2016, **16**, 10–34.
8 J. Nilsson, M. Evander, B. Hammarström and T. Laurell, *Anal. Chim. Acta*, 2009, **649**, 141–157.
9 F. Petersson, L. Åberg, A. M. Swärd-Nilsson and T. Laurell, *Anal. Chem.*, 2007, **79**, 5117–5123.
10 V. Hajko, *Energy Stud. Rev.*, 2013, **20**, 1–23.
11 W. Zhao, R. Cheng, J. R. Miller and L. Mao, *Adv. Funct. Mater.*, 2016, **26**, 3916–3932.
12 C. G. Yang, Z. R. Xu and J. H. Wang, *TrAC, Trends Anal. Chem.*, 2010, **29**, 141–157.
13 M. Tanyeri, M. Ranka, N. Sittipolkul and C. M. Schroeder, *Lab Chip*, 2011, **11**, 1786–1794.
14 D. Wlodkowic, S. Faley, M. Zagnoni, J. P. Wikswo and J. M. Cooper, *Anal. Chem.*, 2009, **81**, 5517–5523.
15 X. Wang, S. Chen, M. Kong, Z. Wang, K. D. Costa, R. A. Li and D. Sun, *Lab Chip*, 2011, **11**, 3656–3662.
16 M. Ozkan, M. Wang, C. Ozkan, R. Flynn, A. Birkbeck and S. Esener, *Biomed. Microdevices*, 2003, **5**, 61–67.
17 A. Kumar, S. J. Williams, H. S. Chuang, N. G. Green and S. T. Wereley, *Lab Chip*, 2011, **11**, 2135–2148.
18 S. Park, C. Pan, T. H. Wu, C. Kloss, S. Kalim, C. E. Callahan, M. Teitell and E. P. Y. Chiou, *Appl. Phys. Lett.*, 2008, **92**, 1–4.
19 S. K. Ravula, D. W. Branch, C. D. James, R. J. Townsend, M. Hill, G. Kaduchak, M. Ward and I. Brener, *Sens. Actuators, B*, 2008, **130**, 645–652.
20 A. Ali-Cherif, S. Begolo, S. Descroix, J. L. Viovy and L. Malaquin, *Angew. Chem., Int. Ed.*, 2012, **51**, 10765–10769.
21 E. Mirowski, J. Moreland, S. E. Russek and M. J. Donahue, *Appl. Phys. Lett.*, 2004, **84**, 1786–1788.
22 A. Ozcelik, J. Rufo, F. Guo, Y. Gu, P. Li, J. Lata and T. J. Huang, *Nat. Methods*, 2018, **15**, 1021–1028.
23 D. J. Collins, C. Devendran, Z. Ma, J. W. Ng, A. Neild and Y. Ai, *Sci. Adv.*, 2016, **2**, e1600089.
24 P. Li and T. J. Huang, *Anal. Chem.*, 2019, **91**(1), 757–767.

25 G. Destgeer, K. H. Lee, J. H. Jung, A. Alazzam and H. J. Sung, *Lab Chip*, 2013, **13**, 4210–4216.
26 M. Wiklund, *Lab Chip*, 2012, **12**, 2018–2028.
27 Z. Mao, P. Li, M. Wu, H. Bachman, N. Mesyngier, X. Guo, S. Liu, F. Costanzo and T. J. Huang, *ACS Nano*, 2017, **11**, 603–612.
28 A. Fakhfouri, C. Devendran, T. Albrecht, D. J. Collins, A. Winkler, H. Schmidt and A. Neild, *Lab Chip*, 2018, **18**, 2214–2224.
29 H. Li, J. R. Friend and L. Y. Yeo, *Biomaterials*, 2007, **28**, 4098–4104.
30 F. Xu, T. D. Finley, M. Turkaydin, Y. Sung, U. A. Gurkan, A. S. Yavuz, R. O. Guldiken and U. Demirci, *Biomaterials*, 2011, **32**, 7847–7855.
31 C. Bouyer, P. Chen, S. Güven, T. T. Demirtaş, T. J. F. Nieland, F. Padilla and U. Demirci, *Adv. Mater.*, 2016, **28**, 161–167.
32 Z. Ma, A. W. Holle, K. Melde, T. Qiu, K. Poeppel, V. M. Kadiri and P. Fischer, *Adv. Mater.*, 2019, **1904181**, 1–6.
33 Y. Bourquin, A. Syed, J. Reboud, L. C. Ranford-Cartwright, M. P. Barrett and J. M. Cooper, *Angew. Chem., Int. Ed.*, 2014, **53**, 5587–5590.
34 A. Marzo and B. W. Drinkwater, *Proc. Natl. Acad. Sci. U. S. A.*, 2019, **116**, 84–89.
35 S. P. Zhang, J. Lata, C. Chen, J. Mai, F. Guo, Z. Tian, L. Ren, Z. Mao, P. H. Huang, P. Li, S. Yang and T. J. Huang, *Nat. Commun.*, 2018, **9**, 2928.
36 J. Shi, D. Ahmed, X. Mao, S.-C. S. Lin, A. Lawit and T. J. Huang, *Lab Chip*, 2009, **9**, 2890.
37 X. Ding, P. Li, S.-C. S. Lin, Z. S. Stratton, N. Nama, F. Guo, D. Slotcavage, X. Mao, J. Shi, F. Costanzo and T. J. Huang, *Lab Chip*, 2013, **13**, 3626.
38 X. Ding, S.-C. S. Lin, B. Kiraly, H. Yue, S. Li, I.-K. Chiang, J. Shi, S. J. Benkovic and T. J. Huang, *Proc. Natl. Acad. Sci. U. S. A.*, 2012, **109**, 11105–11109.
39 G. Kunti, J. Dhar, A. Bhattacharya and S. Chakraborty, *Phys. Fluids*, 2019, **31**, 092003.
40 U. N. Lee, J. H. Day, A. J. Haack, R. C. Bretherton, W. Lu, C. A. DeForest, A. B. Theberge and E. Berthier, *Lab Chip*, 2020, **20**, 525–536.
41 A. H. Meng, N. T. Nguyen and R. M. White, *Biomed. Microdevices*, 2000, **2**, 169–174.
42 N. T. Nguyen and R. M. White, *Sens. Actuators, A*, 1999, **77**, 229–236.
43 R. K. Vadivelu, H. Kamble, M. J. A. Shiddiky and N. T. Nguyen, *Micromachines*, 2017, **8**, 1–23.
44 Y. Wu, Z. Ao, B. Chen, M. Muhsen, M. Bondesson, X. Lu and F. Guo, *Nanotechnology*, 2018, **29**, 50400.
45 V. GiurGiutiu, *Structural Health Monitoring with Piezoelectric Wafer Active Sensors*, 1st edn, 2007.
46 P.-H. Huang, N. Nama, Z. Mao, P. Li, J. Rufo, Y. Chen, Y. Xie, C.-H. Wei, L. Wang and T. J. Huang, *Lab Chip*, 2014, **14**, 4319–4323.
47 D. Bodas and C. Khan-Malek, *Sens. Actuators, B*, 2007, **123**, 368–373.
48 H. Bachman, P. H. Huang, S. Zhao, S. Yang, S. P. Zhang, H. Fu and T. J. Huang, *Lab Chip*, 2018, **18**, 433–441.
49 H. Bachman, H. Fu, P.-H. Huang, Z. Tian, J. Embry-Seckler, J. Rufo, Z. Xie, J. H. Hartman, S. Zhao, S. Yang, J. N. Meyer and T. J. Huang, *Lab Chip*, 2019, **19**, 2404–2414.
50 Z. Wang, P.-H. Huang, C. Chen, H. Bachman, S. Zhao, S. Yang and T. J. Huang, *Lab Chip*, 2019, **19**, 4021–4032.
51 L. Y. Yeo and J. R. Friend, *Annu. Rev. Fluid Mech.*, 2014, **46**, 379–406.
52 H. Bruus, *Lab Chip*, 2012, **12**, 20–28.
53 J. Chen, Z. Su and L. Cheng, *Smart Mater. Struct.*, 2010, **19**, 015004.